Cell Metabolism
Article

The Hypoxia-Inducible MicroRNA Cluster miR-199a∼214 Targets Myocardial PPARδ and Impairs Mitochondrial Fatty Acid Oxidation

Hamid el Azzouzi,[1,4,14] Stefanos Leptidis,[1,5,14] Ellen Dirkx,[1,14] Joris Hoeks,[2] Bianca van Bree,[2] Karl Brand,[6,7] Elizabeth A. McClellan,[7] Ella Poels,[1] Judith C. Sluimer,[3] Maarten M.G. van den Hoogenhof,[8] Anne-Sophie Armand,[9] Xiaoke Yin,[10] Sarah Langley,[10] Meriem Bourajjaj,[5] Serve Olieslagers,[1] Jaya Krishnan,[11] Marc Vooijs,[12] Hiroki Kurihara,[13] Andrew Stubbs,[7] Yigal M. Pinto,[8] Wilhelm Krek,[11] Manuel Mayr,[10] Paula A. da Costa Martins,[1] Patrick Schrauwen,[2] and Leon J. De Windt[1,*]

[1]Department of Cardiology, CARIM School for Cardiovascular Diseases
[2]Department of Human Biology, NUTRIM School for Nutrition, Toxicology and Metabolism
[3]Department of Pathology, CARIM School for Cardiovascular Diseases
Maastricht University, 6229 ER Maastricht, the Netherlands
[4]Department of Cardiology, University Medical Center Utrecht, 3584 CX Utrecht, the Netherlands
[5]Interuniversity Cardiology Institute Netherlands, Royal Netherlands Academy of Sciences, 3511 GC Utrecht, the Netherlands
[6]Department of Cardiology
[7]Department of Bioinformatics
Erasmus University Medical Center, 3015 CE Rotterdam, the Netherlands
[8]Heart Failure Research Centre, Academic Medical Center, 1105 AZ Amsterdam, the Netherlands
[9]Centre d'Etude de la Sensori-motricité, UMR 8194 CNRS, Université Paris Descartes, 75270 Paris Cedex, France
[10]King's BHF Centre, King's College London, London WC2R 2LS, UK
[11]Institute of Molecular Health Sciences, ETH Zurich, 8092 Zurich, Switzerland
[12]Department of Radiation Oncology (MAASTRO lab), Maastricht University Medical Centre, 6202 AZ Maastricht, the Netherlands
[13]Department of Physiological Chemistry and Metabolism, University of Tokyo, Tokyo 113-8654, Japan
[14]These authors contributed equally to this work
*Correspondence: l.dewindt@maastrichtuniversity.nl
http://dx.doi.org/10.1016/j.cmet.2013.08.009

SUMMARY

Peroxisome proliferator-activated receptor δ (PPARδ) is a critical regulator of energy metabolism in the heart. Here, we propose a mechanism that integrates two deleterious characteristics of heart failure, hypoxia and a metabolic shift toward glycolysis, involving the microRNA cluster *miR-199a∼214* and PPARδ. We demonstrate that under hemodynamic stress, cardiac hypoxia activates *DNM3os*, a noncoding transcript that harbors the microRNA cluster *miR-199a∼214*, which shares PPARδ as common target. To address the significance of *miR-199a∼214* induction and concomitant PPARδ repression, we performed antagomir-based silencing of both microRNAs and subjected mice to biomechanical stress to induce heart failure. Remarkably, antagomir-treated animals displayed improved cardiac function and restored mitochondrial fatty acid oxidation. Taken together, our data suggest a mechanism whereby *miR-199a∼214* actively represses cardiac PPARδ expression, facilitating a metabolic shift from predominant reliance on fatty acid utilization in the healthy myocardium toward increased reliance on glucose metabolism at the onset of heart failure.

INTRODUCTION

Despite the remarkable metabolic flexibility of the heart regarding nutritional status and cardiac demand, several studies demonstrated abnormalities in cardiac lipid homeostasis and energy production as a consistent feature of heart failure (HF) (Barger and Kelly, 2000; Razeghi et al., 2001). Due to limited oxygen and fatty acid availability, the fetal heart mainly relies on anaerobic glucose utilization. In contrast, rising cardiac work and the abundance of fatty acids in the postnatal heart bring about increased reliance on mitochondrial fatty acid oxidation (FAO). Hemodynamically stressed hearts exhibit a return to the fetal metabolic pattern that is hallmarked by impaired mitochondrial FAO and a shift to further reliance on glucose metabolism (Rajabi et al., 2007; Razeghi et al., 2001). Due to the strict aerobic nature of the heart and the inability to generate sufficient energy under anaerobic conditions, reliance on glycolysis has a major impact on available ATP levels (Di Lisa et al., 2007). As such, hypoxia is considered to be a characteristic of the failing heart (Giordano, 2005; Sabbah et al., 2000; Tanaka et al., 1994).

Regulation of the metabolic profile by activity of the peroxisome proliferator-activated receptor δ (PPARδ) has been shown to play a role in the metabolic switch from FAO to glycolysis (Burkart et al., 2007). Heart muscle-restricted deletion of PPARδ resulted in progressive lipid accumulation, cardiac hypertrophy, and congestive heart failure (Cheng et al., 2004). Conversely, selective overexpression of PPARδ in the mouse heart provoked an increase in myocardial glucose utilization with no myocardial

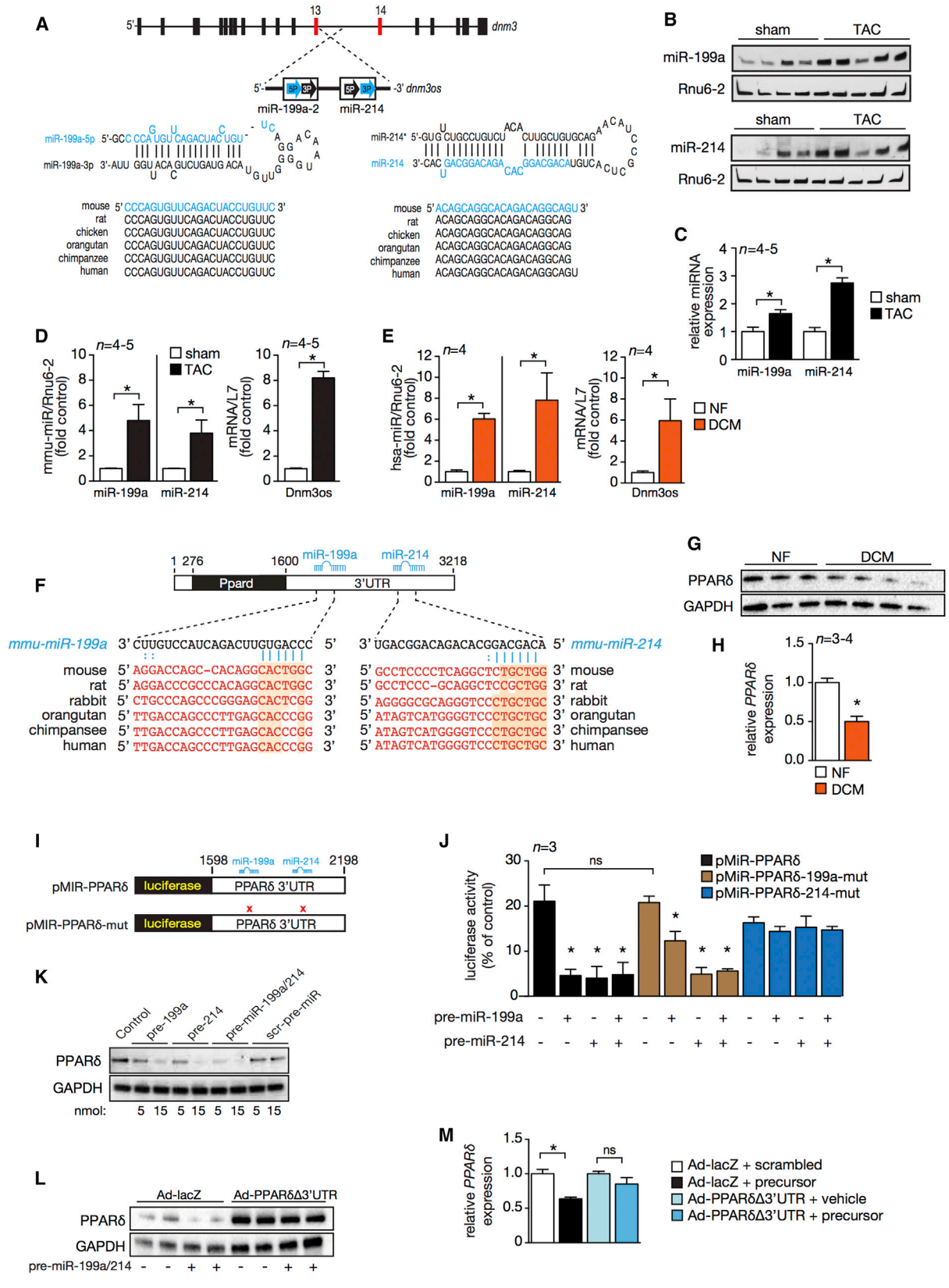

(legend on next page)

lipid accumulation due to preserved FAO and resistance to cardiac disease induced by ischemia reperfusion injury (Burkart et al., 2007). These studies clearly illustrate the importance of PPARδ signaling in energy homeostasis and pathogenesis of heart failure. Despite this, whether and how PPARδ is regulated remains unclear.

Small noncoding RNAs (~18–24 nucleotides), such as microRNAs (miRNAs, miRs), have been shown to be a fascinating mechanism, coordinating complex programs of gene expression (da Costa Martins et al., 2008; Thum et al., 2007; van Rooij et al., 2007). By regulating the stability and translation of messenger RNAs by base-pairing with the 3′ UTRs, miRNAs have been shown to impact gene expression in cardiovascular disease (da Costa Martins et al., 2008; Thum et al., 2007). In a comparative study among animal models of pathological cardiac remodeling, *miR-199a* and *miR-214* showed increased expression in these animal models as well as in samples of failing human hearts (van Rooij et al., 2006). In addition, expression of these miRNAs induced a hypertrophic response in cardiomyocytes, suggesting that *miR-199a* and *miR-214* are involved in the processes leading to cardiac disease (van Rooij et al., 2006). Despite their apparent role in cardiac remodeling, the mechanisms driving the regulation of *miR-199a* and *miR-214* in the failing heart and how these miRNAs provoke deleterious cardiac remodeling remain undefined.

We report here that the miRNA cluster *miR-199a~214*, embedded in chromosome 1 in a large noncoding RNA, *Dnm3os*, actively represses PPARδ. Furthermore, myocardial hypoxia provokes *Dnm3os* activation and concomitant *miR-199a~214* expression. Increased expression of *miR-199a* and *miR-214* promotes decreased cardiac PPARδ expression, mitochondrial disarray and I band widening, and decreased mitochondrial fatty acid oxidative capacity. Conversely, antagomir-based silencing of *miR-199a~214* in mice subjected to pressure overload derepressed cardiac PPARδ levels, normalized mitochondrial fatty acid oxidation, and improved cardiac structure and function. Taken together, our data suggest a mechanism whereby myocardial hypoxia, a hallmark of heart failure, induces expression of members of the miRNA cluster *miR-199a~214*, which actively downregulate cardiac PPARδ expression, provoking a switch toward a mitochondrial glycolytic metabolic profile that contributes to characteristics of heart failure.

RESULTS

The miR-199a:214 Cluster Is Increased in Human and Mouse Heart Failure

Recent cardiac microRNA profiling studies from our group and others have shown that the expression of both *miR-199a* and *miR-214* is increased in various models of heart failure (da Costa Martins et al., 2010; Leptidis et al., 2013; van Rooij et al., 2006). Human *miR-199a~214* is encoded by a large noncoding RNA, *DNM3os*, which is transcribed in the opposite strand of the *DNM3* gene (Figure 1A). Both mature miRNAs, *hsa-miR-199a-2-5p* and *hsa-miR-214-3p*, are evolutionary conserved among several species (Figure 1A). Northern blot analysis confirmed that both *miR-199a* and *miR-214* are upregulated in hearts from mice subjected to pressure overload by transverse aortic constriction (TAC) (Figures 1B and 1C). Quantitative RT-PCR also showed an increase in *DNM3os* expression in TAC-operated mice, verifying the clustered expression of both miRs in failing mouse hearts (Figure 1D). An increased expression of *DNM3os*, along with the encoded miRNA cluster *miR-199a~214*, was also evident in biopsies of cardiac tissue from heart failure patients (Figure 1E).

Mechanistically, *miR-199a* and *miR-214* are predicted to target multiple genes according to several public data sets. Interestingly, we identified PPARδ as a predicted common target of both microRNAs. Indeed, investigation of the 3′ UTR of PPARδ revealed an evolutionarily conserved seed region for *miR-214* in both human and mouse PPARδ and a less-conserved seed region for *miR-199a* (Figure 1F). Next, we examined whether PPARδ levels are affected in biopsies of cardiac tissue from heart failure patients. Western blot analysis in biopsies of cardiac tissue from heart failure patients showed lower protein levels of PPARδ compared with human control heart tissue (Figures 1G and 1H).

To further confirm the functionality of the seed regions of *miR-199a* and *miR-214*, we fused the 3′ UTR of PPARδ to a luciferase

Figure 1. Expression of the *miR-199a~214* Cluster Targets PPARδ

(A) Schematic representation of genomic localization and precursor of *hsa-miR-199a* and *hsa-miR-214*, encoded by the large noncoding RNA *DNM3os*, located on the opposite strand in intron 14 of the dynamin-3 (DNM3) gene, on chromosome 1 in the human genome. The mature *miR-199a* and *miR-214* strands are phylogenetically conserved.

(B) Northern blot analysis of *miR-199a* and *miR-214* expression in hearts from sham mice or mice subjected to transverse aortic constriction (Bourajjaj et al., 2008). *Rnu6-2* was used as a loading control.

(C) Quantification of *Rnu6-2*-corrected northern blot signals for *miR-199a* and *miR-214* from (B).

(D and E) Real-time PCR analysis of transcript abundance for *miR-199a*, *miR-214*, and *DNM3os* in hearts from sham mice and mice subjected to TAC (D) and in nonfailing and dilated cardiomyopathy (DCM) patient-derived left ventricular myocardium (E).

(F) Location of *miR-199a* and *miR-214* seed regions in human and mouse PPARδ 3′ UTR.

(G) Western blot analysis of endogenous PPARδ and GAPDH in nonfailing and dilated cardiomyopathy patient-derived left ventricular myocardium.

(H) Quantification of GAPDH-corrected protein levels of PPARδ from (G).

(I) Schematic representation of luciferase reporter constructs harboring intact or mutated PPARδ 3′ UTR.

(J) Activity assay of luciferase reporter constructs harboring intact PPARδ 3′ UTR or mutated seed regions for either *miR-199a* or *miR-214*, after transfection with synthetic precursor for *miR-199a* and/or with *miR-214*. A scrambled miRNA precursor was used as a control.

(K) Western blot analysis of endogenous PPARδ and GAPDH in neonatal rat cardiomyocytes transfected with synthetic precursor for *miR-199a* and/or with *miR-214*. Transfection with scrambled synthetic precursor was used as a negative control.

(L) Western blot analysis of endogenous PPARδ and GAPDH in neonatal rat cardiomyocytes infected with control adenovirus harboring the lacZ gene (Ad-lacZ) or adenovirus lacking the 3′ UTR of PPARδ (Ad-PPARδ-Δ3′ UTR), with or without transfection of synthetic precursors for *miR-199a* and *miR-214*. *$p < 0.05$ versus corresponding control group; #$p < 0.05$ versus corresponding experimental group (error bars are SEM). See also Figure S1.

reporter gene, generating miRNA expression reporter constructs (Figure 1I). Coexpression of synthetic *miR-199a* and/or *miR-214* decreased PPARδ 3′ UTR reporter activity (Figure 1J), while mutating the seed regions for *miR-214* in the PPARδ 3′ UTR reporter construct abrogated the inhibitory effect of *miR-214* and *miR-199a*. Mutating the seed region for *miR-199a* only had an inhibitory effect on *miR-199a* transfection (Figure 1J; Figure S1A available online), indicating a dominant effect of *miR-214* on PPARδ repression and establishing the causative link between posttranslational control by the miRNA cluster *miR-199a∼214* on PPARδ. To further verify whether increased *miR-199a∼214* levels are directly responsible for the decrease of PPARδ protein levels in the failing hearts, we overexpressed synthetic precursors for *miR-199a* and/or *miR-214* in a dose-dependent manner and observed efficient downregulation of endogenous PPARδ expression (Figure 1K). Finally, we overexpressed a form of PPARδ lacking a 3′ UTR and demonstrated that this form of PPARδ was insensitive to precursor transfection of *miR-199a* and *miR-214* (Figures 1L and 1M). Taken together, these data demonstrate that *miR-199a* and *miR-214*, as well as their host gene *Dnm3os*, are increased in human and mouse heart failure and directly target PPARδ.

Hypoxia Drives the Expression of *miR-199a∼214* through Hif1α/Twist1

Myocardial hypoxia has been associated with a variety of clinical conditions, including ischemic heart disease (IHD), systemic hypertension, and pathological cardiac hypertrophy, where the hypoxia-inducible transcription factor 1α (Hif1α) drives hypoxia-inducible gene expression (Lei et al., 2008; Rey and Semenza, 2010). One Hif1α downstream mechanism employs the activation of the transcription factor Twist1 by binding directly to the hypoxia response element (HRE) in the Twist1 proximal promoter (Yang et al., 2008). Interestingly, *DNM3os* has been identified as a target gene for the helix-loop-helix transcription factor Twist1 (Loebel et al., 2005). To verify the functionality of this element, a luciferase reporter harboring the proximal DNM3os promoter region was generated and tested for Hif1α or Twist1 sensitivity (Figure 2A). The DNM3os-luc reporter demonstrated activation upon cotransfection with Hif1α or Twist1, while the enhancer box (E box)-mutated DNM3os-luc reporter construct showed no activation under the same conditions (Figure 2B).

Dnm3os homozygous-deficient mice die within 1 month of birth accompanied by skeletal abnormalities, defects in dorsal neural arches and spinous processes of the vertebrae, osteopenia, and reduced expression of its host genes *miR-199a* and *miR-214* (Watanabe et al., 2008). We reasoned that *Dnm3os*-deficient hearts may display derepression of PPARδ due to the reduced expression of *miR-199a∼214*. In line, western blotting demonstrated increased PPARδ expression in Dnm3os-deficient hearts compared to hearts from wild-type (WT) littermates (Figures 2C and 2D). The premature death of juvenile *Dnm3os*-deficient mice precluded further functional studies.

The PPARδ 3′ UTR reporter also showed strong inhibition of luciferase activity under hypoxia, with peak activity on day 3 (Figure 2E), confirming both the hypoxia-sensitive and microRNA-mediated posttranslational regulation of PPARδ. Quantitative RT-PCR confirmed a significant increase of endogenous *miR-199a*, *miR-214*, and *Dnm3os* transcript abundance in cardiomyocytes upon exposure to hypoxia (2% O_2) (Figure 2F), indicating hypoxia as a primary stimulus for the expression of mature *miR-199a* and *miR-214* via transcriptional regulation of *DNM3os*. Locked nucleotide acid (LNA) knockdown probes for *miR-199a* and/or *miR-214* exhibited a strong and specific repression of the target miRs as quantified by PCR (Figures S1B and S1C). LNA-based knockdown of *miR-199a* and *miR-214* inhibited the hypoxia-mediated PPARδ downregulation (Figure 2G). Interestingly, knockdown of *miR-214* abrogated the hypoxia-induced downregulation of PPARδ more effectively than when *miR-199a* was targeted (Figure 2G). These results indicate a more pronounced role for *miR-214* than *miR-199a* in hypoxia-mediated knockdown of PPARδ. Ventricular deletion of Hif1α in mice was previously used to implicate a Hif1α-PPARγ axis in hypertrophy-induced PPARγ activation, metabolic reprogramming, and contractile dysfunction (Krishnan et al., 2009). Accordingly, we tested whether cardiac-specific Hif1α deletion would also abrogate PPARδ expression under baseline conditions or after pressure overload. Western blotting demonstrated that PPARδ expression was reduced after pressure overload, and this reduction was efficiently prevented by cardiac-specific Hif1α deletion (Figures 2H and 2I). In conclusion, the data demonstrate that hypoxia serves as an upstream stimulus for *Dnm3os* and *miR-199a∼214* expression in the heart in a hypoxia- and/or Hif1α-dependent manner.

Conditional Targeted Deletion of PPARδ Causes Severe Cardiac Dysfunction

To investigate whether maintenance of PPARδ expression is required for normal myocardial homeostasis and to bypass the early embryonic lethality of PPARδ null mice (Barak et al., 2002), we provoked deletion of a floxed PPARδ ($PPAR\delta^{F/F}$) allele using a tamoxifen-inducible Cre recombinase under the control of the cardiac-specific α-myosin heavy-chain promoter (αMHC). Specificity of PPARδ gene deletion was shown by real-time RT-PCR for all three endogenous PPAR isoforms, demonstrating that our genetic intervention did not affect PPARα or PPARγ transcripts, but resulted in a strong and selective downregulation of PPARδ transcripts (Figure S2A). We forced PPARδ gene deletion at the age of 8 weeks and noted that within 5 days after tamoxifen delivery, αMHC-MCM-$PPAR\delta^{F/F}$ mice displayed signs of inactivity and a weak condition compared to all control groups. Indeed, up to 25% of tamoxifen-treated αMHC-MCM-$PPAR\delta^{F/F}$ mice died within 1 week after initiation of the treatment, and this mortality rate increased to 75% during the following 2 weeks (data not shown). Upon autopsy, tamoxifen-treated αMHC-MCM-$PPAR\delta^{F/F}$ displayed severely enlarged hearts (Figure S2B).

Cardiac tissue from these mice revealed intricate features of clinical heart failure, including hypertrophied myofibers, myocyte disarray, and interstitial fibrosis in hearts (Figure S2B), which was reflected by doubling of heart weight at the whole-organ level (Figure S2C). These data demonstrate that conditional cardiac-specific deletion of PPARδ in the adult heart causes rapid cardiac remodeling, which results in multiple clinical signs of end-stage heart failure and reduced survivability. Cardiac geometry and function was assessed noninvasively by echocardiography at 2 weeks after tamoxifen treatment (Figure S2D; Table S1). At this time point, tamoxifen-treated αMHC-MCM-$PPAR\delta^{F/F}$

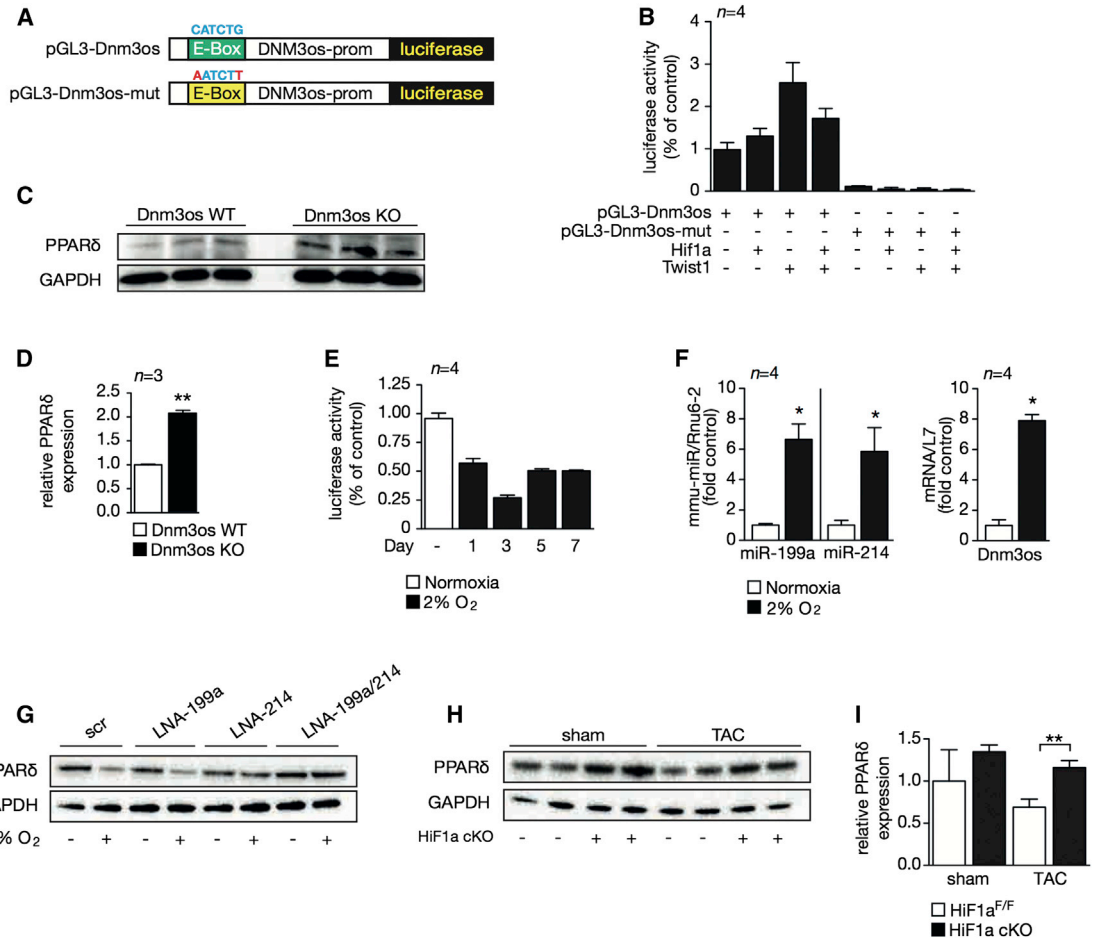

Figure 2. Hypoxia Regulates Expression of the *miR-199a∼214* Cluster

(A) Schematic representation of luciferase reporter constructs harboring intact or mutated proximal *DNM3os* promoter region.

(B) Activity assay of luciferase reporter construct, driven by the *DNM3os* promoter after induction of Hif1α or Twist1 expression, in HEK 293 cells.

(C) Western blot analysis of endogenous PPARδ and GAPDH in WT and Dnm3os knockout (KO) mice.

(D) Quantification of GAPDH-corrected protein levels of PPARδ from (C).

(E) Activity assay of a PPARδ 3′ UTR luciferase reporter construct in HEK 293 cells exposed to hypoxic conditions (2% O_2) for the annotated periods.

(F) Real-time PCR analysis of transcript abundance for *miR-199a*, *miR-214*, and *DNM3os*.

(G) Western blot analysis of endogenous PPARδ and GAPDH in neonatal rat cardiomyocytes transfected with scrambled LNA control (scr), LNA against miR-199a (LNA 199a), LNA against miR-214 (LNA 214), or both LNA against miR-199a and LNA against miR-214 (LNA 199a/214) and exposed to a hypoxic environment (2% O_2) for 3 days.

(H) Western blot analysis of endogenous PPARδ and GAPDH in WT and Hif1α KO mice.

(I) Quantification of GAPDH-corrected protein levels of PPARδ from (H). *p < 0.05 versus corresponding control group; #p < 0.05 versus corresponding experimental group (error bars are SEM). See also Figure S1.

animals demonstrated a significant decline in cardiac contractility, as evidenced by a 50% decrease in fractional shortening (Figure S2E), and severe left ventricular dilation (Figure S2F). These data indicate that conditional cardiac-specific deletion of PPARδ provoked progressive functional and geometrical deterioration consistent with a heart failure phenotype, including potent reactivation of stress-induced embryonic genes such as *Acta1*, *Nppb*, *Myh7*, and *Nppa* (Figure S2G). Moreover, we noted a substantial decrease in transcript abundance for *Cd36* and *hadha*, without changes in *Slc2a1* transcript abundance (Figure S2H), indicating a reduction in fatty acid transport capacity and oxidation. Conclusively, deletion of PPARδ in the adult heart induces rapid and spontaneous cardiac dysfunction, induction of fetal hypertrophic marker genes, and selective downregulation of genes involved in fatty acid metabolism.

miR-214 Silencing Improves Cardiac Contractility and Derepresses PPARδ

Antagomirs are RNA-like oligonucleotides that are reverse compliment to mature microRNAs and harbor various modifications for ribonuclease (RNase) protection and pharmacologic properties such as enhanced tissue and cellular uptake. Antagomirs efficiently silence microRNAs in most tissues in vivo (Krützfeldt et al., 2005). To intervene in the targeted downregulation of PPARδ by *miR-199a∼214* in cardiac disease conditions, we subjected mice to transverse aortic constriction pressure overload

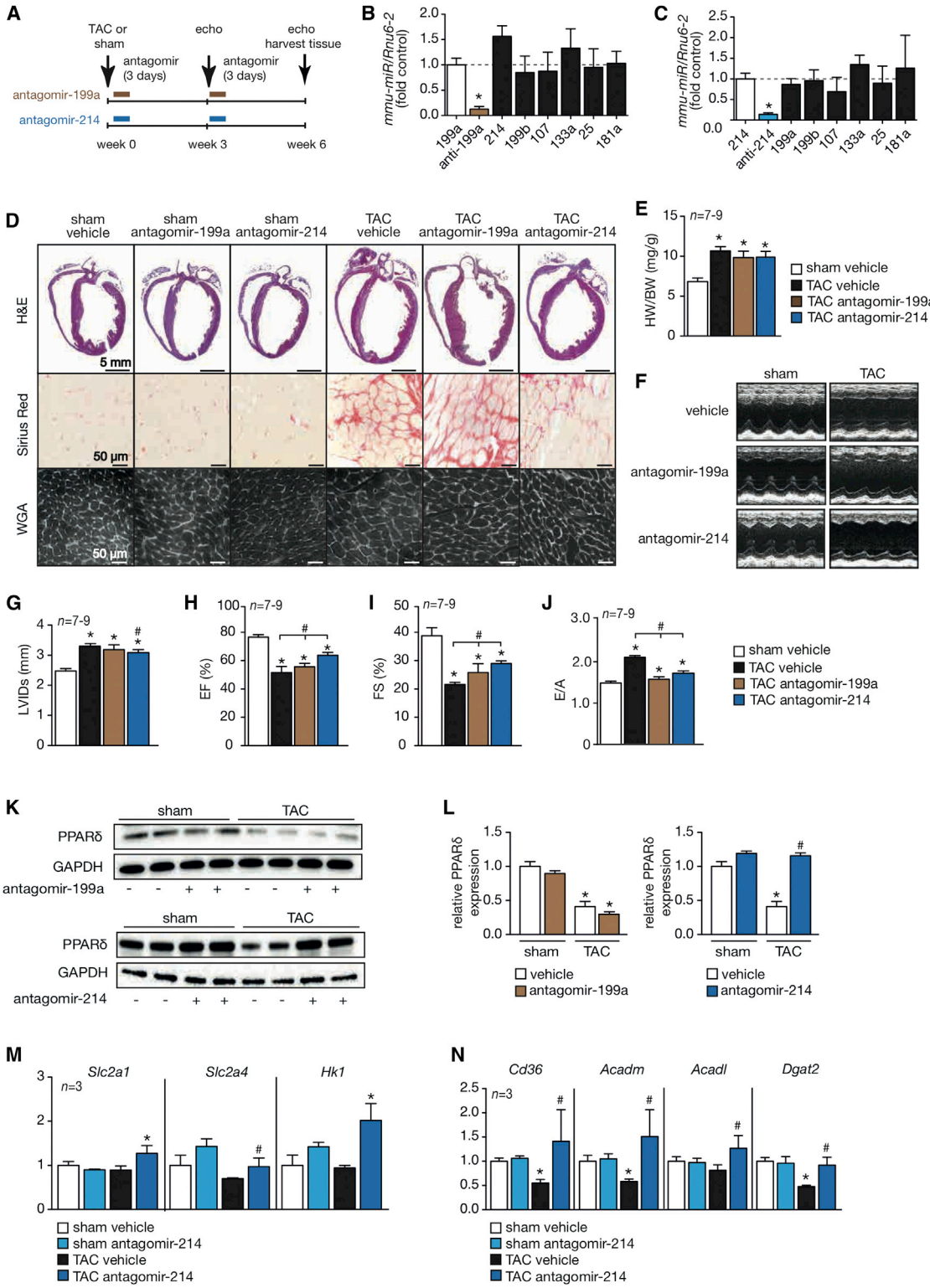

Figure 3. Silencing *miR-214* or *miR-199a* Differentially Improves Cardiac Dysfunction

(A) Design of antagomir treatment study.

(B) Quantitative RT-PCR analysis of *miR-199a*, *miR-214*, *miR-199b*, *miR-107*, *miR-133a*, *miR-25*, and *miR-181a* expression in mice hearts after vehicle or antagomir-199a treatment.

(C) Quantitative RT-PCR analysis of *miR-199a*, *miR-214*, *miR-199b*, *miR-107*, *miR-133a*, *miR-25*, and *miR-181a* expression in mice hearts after vehicle or antagomir-214 treatment.

(legend continued on next page)

Table 1. Morphometric and Echocardiographic Characteristics of Wild-Type Mice Treated with Vehicle, Antagomir-199a, or Antagomir-214 and Subjected to Sham or Transverse Aortic Constriction Surgery

	Sham			TAC		
	Vehicle	Antagomir-199a	Antagomir-214	Vehicle	Antagomir-199a	Antagomir-214
n	8	7	8	8	8	9
BW (g)	29 ± 1	27 ± 1	26 ± 1	26 ± 1	29 ± 1	28 ± 1
LV mass (mg)	98 ± 4	102 ± 8	102 ± 8	130 ± 6*	155 ± 12*#	139 ± 10*
LV mass/BW (mg/g)	3.50 ± 0.18	3.80 ± 0.30	3.96 ± 0.58	4.95 ± 0.20*	5.49 ± 0.48*	5.07 ± 0.33*
IVSd (mm)	0.86 ± 0.04	0.90 ± 0.04	0.89 ± 0.06	0.99 ± 0.07*	1.07 ± 0.05*	0.99 ± 0.04*
IVSs (mm)	1.31 ± 0.11	1.30 ± 0.08	1.25 ± 0.06	1.32 ± 0.08	1.46 ± 0.08*	1.35 ± 0.06
LVIDd (mm)	3.86 ± 0.11	3.69 ± 0.13	3.81 ± 0.08	4.19 ± 0.05*	4.07 ± 0.14*	4.24 ± 0.13*
LVIDs (mm)	2.36 ± 0.08	2.41 ± 0.15	2.62 ± 0.11	3.30 ± 0.08*	3.07 ± 0.17*	3.01 ± 0.15*
LVPWd (mm)	0.91 ± 0.07	1.00 ± 0.09	0.93 ± 0.09	0.94 ± 0.07	1.17 ± 0.11*	1.00 ± 0.06
LVPWs (mm)	1.33 ± 0.06	1.37 ± 0.09	1.34 ± 0.09	1.18 ± 0.08	1.41 ± 0.10#	1.30 ± 0.05#
EF (%)	77 ± 1	75 ± 3	72 ± 2	51 ± 5*	56 ± 4*	64 ± 2*#
FS (%)	39 ± 4	38 ± 3	35 ± 2	21 ± 1*	25 ± 3*	29 ± 1*#
E/A (mm/s)	1.45 ± 0.08	1.57 ± 0.12	1.58 ± 0.13	2.04 ± 0.13*	1.58 ± 0.14#	1.72 ± 0.13#

Data are expressed as means ± SEM. TAC, transverse aortic constriction; sham, sham-operated control group; BW, body weight; LV, left ventricular; IVSd, interventricular septal thickness at end diastole; IVSs, interventricular septal thickness at end systole; LVIDd, left ventricular internal dimension at end diastole; LVIDs, left ventricular internal dimension at end systole; LVPWd, left ventricular posterior wall thickness at end diastole; LVPWs, left ventricular posterior wall thickness at end systole; EF, ejection fraction; FS, fractional shortening; E/A, Doppler E/A ratio.*$p < 0.05$ versus sham group treated with control antagomir; #$p < 0.05$ versus experimental group.

for 6 weeks and treated them with antagomirs for either *miR-199a* or *miR-214* for 3 consecutive days at 3-week intervals (Figure 3A). To verify silencing efficiency of antagomir-199a and antagomir-214, quantitative RT-PCR was performed (Figures 3B and 3C). The specificity of the antagomirs used was verified by measuring the expression of other microRNAs (Figures 3B and 3C). Sham-operated mice treated with vehicle, antagomir-199a, antagomir-214 showed no signs of histopathology or alterations in heart size (Figures S3A–S3C). Vehicle-treated mice showed substantial cardiac enlargement, displayed hypertrophied myofibers, myocyte disarray, and interstitial fibrosis upon hemodynamic stress (Figure 3D), and displayed significantly increased heart weights (Figure 3E). No significant reduction in heart weight was observed in antagomir-199a- or antagomir-214-treated mice that underwent TAC surgery (Figures 3D and 3E). Antagomir-199a- or antagomir-214-treated pressure-overloaded hearts displayed less hypertrophied myofibers, myocyte disarray, and reduced fibrosis, with the effects more pronounced for mice treated with antagomir-214 (Figure 3D). Analysis of cardiac function by M-mode echocardiography at 6 weeks demonstrated an increase in left ventricular internal diameter (LVID) in mice subjected to pressure overload and treated with vehicle, which was slightly reduced upon antagomir-214 treatment (Figures 3F and 3G). Importantly, the decrease in systolic and diastolic contractility observed in vehicle-treated mice subjected to TAC surgery was significantly improved by either antagomir-199a or antagomir-214 treatment (Figures 3H–3J; Table 1). Furthermore, antagomir-214 treatment was able to fully derepress PPARδ levels following hemodynamic stress (Figures 3K and 3L). To analyze the effect of antagomir-214 treatment on metabolism, we performed RT-PCRs for both fatty acid and glucose marker genes. Cardiac pressure overload did not alter the expression of genes implicated in glucose metabolism (Figure 3M). In contrast, pressure overload induced a pronounced reduction in key genes involved in fatty acid metabolism, including *acyl-coenzyme A dehydrogenase, medium-chain* (*Acadm*), *CD36 antigen* (*Cd36*), and *diacylglycerol O-acyltransferase 2* (*Dgat2*), which were fully restored upon antagomir-214 treatment (Figure 3N). Antagomir-214 treatment did not influence the reactivation of stress-induced fetal genes, including *Nppa*, *Nppb*, *Acta1*, and *Myh7* (Figure S3D). Taken together, these data demonstrate that single *miR-199a* or *miR-214*

(D) Representative images of H&E (top panels), Sirius red-stained (middle panels), or WGA-labeled (lower panels) histological sections of mice hearts after 6 weeks of sham or TAC surgery, treated with vehicle or antagomirs.
(E) Gravimetric analysis of corrected heart weights of mice after 6 weeks of sham or TAC surgery, treated with vehicle or antagomirs.
(F) Representative M-mode images in mice hearts after 6 weeks of sham or TAC surgery, treated with vehicle or antagomirs.
(G–J) Quantification by echocardiography of LV internal diameter at systole (LVIDs) (G), ejection fraction (EF) (H), fractional shortening (%FS) (I), and early-to-late ventricular filling velocity (E/A) (J) of mice hearts after 6 weeks of sham or TAC surgery, treated with vehicle or antagomirs.
(K) Western blot analysis of endogenous PPARδ and GAPDH levels in mice hearts after 6 weeks of sham or TAC surgery, treated with vehicle, antagomir-199a, or antagomir-214.
(L) Quantification of GAPDH-corrected protein levels of PPARδ.
(M and N) Real-time PCR analysis of transcript abundance for glucose metabolism marker genes (M) and fatty acid metabolism marker genes (N) in mice hearts after 6 weeks of sham or TAC surgery, treated with vehicle or antagomirs. *$p < 0.05$ versus corresponding control group; #$p < 0.05$ versus corresponding experimental group (error bars are SEM). See also Figure S3.

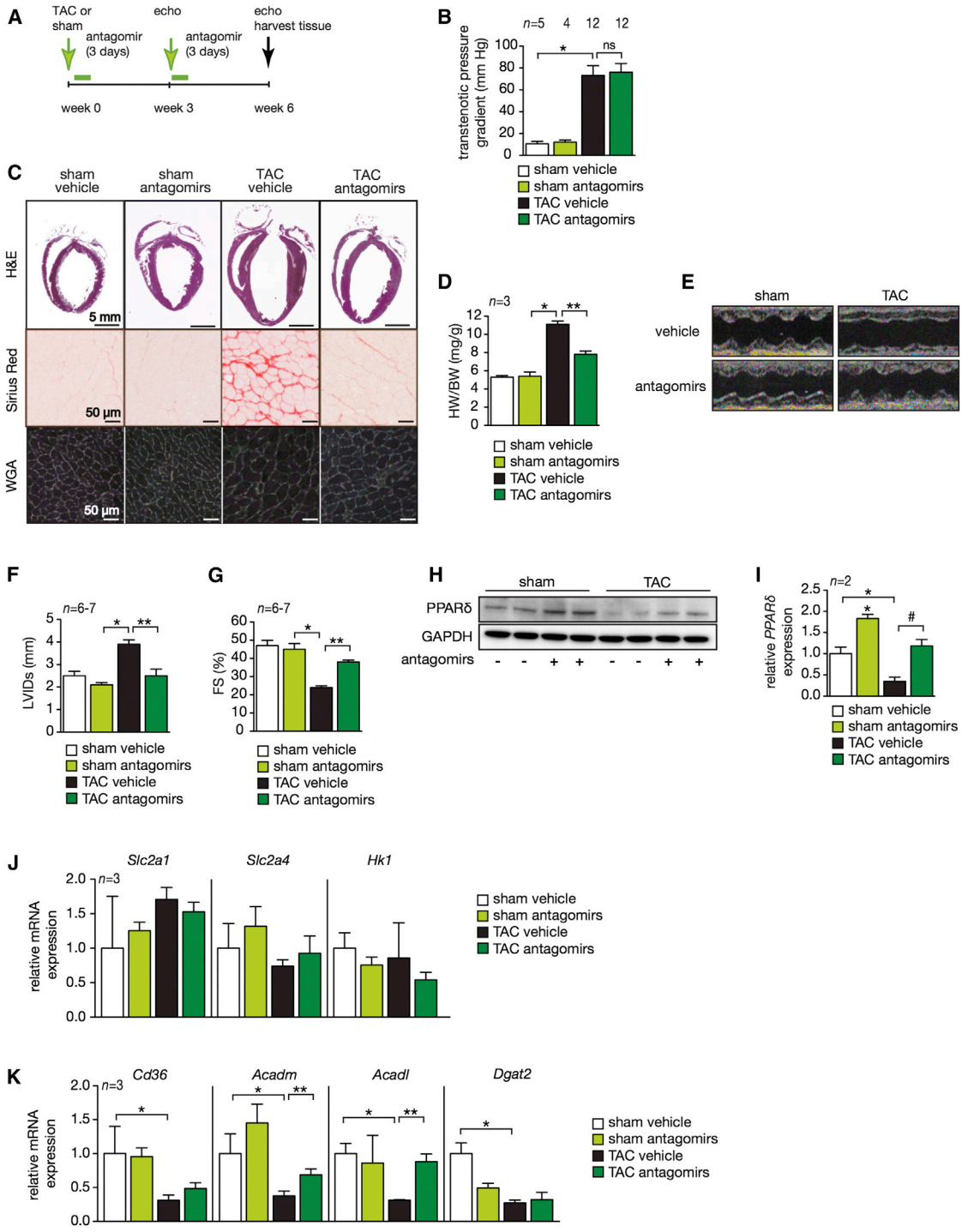

Figure 4. Antagomir-Mediated Silencing of Both *mir-199a* and *miR-214* Attenuates Cardiac Remodeling

(A) Design of antagomir treatment study.

(B) Pressure gradients across the transverse aorta measured noninvasively to validate the TAC procedure.

(C) Representative images of H&E (top panels), Sirius red-stained (middle panels), or WGA-labeled (lower panels) histological sections of mice hearts after 6 weeks of sham or TAC surgery, treated with vehicle or antagomirs.

(D) Gravimetric analysis of corrected heart weights of mice after 6 weeks of sham or TAC surgery, treated with vehicle or antagomirs.

(E) Representative M-mode images in mice hearts after 6 weeks of sham or TAC surgery, treated with vehicle or antagomirs.

(F and G) Quantification by echocardiography of LV internal diameter at systole (LVIDs) (F) and fractional shortening (%FS) (G) of mice hearts after 6 weeks of sham or TAC surgery, treated with vehicle or antagomirs.

(H) Western blot analysis of endogenous PPARδ and GAPDH levels in mice hearts after 6 weeks of sham or TAC surgery, treated with vehicle or antagomirs.

(legend continued on next page)

Table 2. Echocardiographic Analysis of Mice Following Sham Operation or Transverse Aortic Constriction with or without Double Antagomir-199a and Antagomir-214 Treatment

	Sham		TAC	
	Vehicle	Antagomir-199a∼214	Vehicle	Antagomir-199a∼214
n	7	6	7	6
IVSd (mm)	0.98 ± 0.10	0.83 ± 0.14	1.29 ± 0.07*	1.23 ± 0.14*
IVSs (mm)	1.79 ± 0.05	1.68 ± 0.07	1.74 ± 0.06	1.98 ± 0.09*#
LVIDs (mm)	2.55 ± 0.22	2.10 ± 0.13	3.75 ± 0.17*	2.52 ± 0.26#
LVIDd (mm)	4.35 ± 0.12	4.12 ± 0.22	4.78 ± 0.14*	4.38 ± 0.18#
LVPWs (mm)	1.80 ± 0.08	2.09 ± 0.08	1.49 ± 0.10	1.97 ± 0.16*
LVPWd (mm)	0.91 ± 0.07	1.27 ± 0.14	1.11 ± 0.07*	1.23 ± 0.08
FS (%)	47 ± 1	45 ± 1	25 ± 1*	38 ± 1*#

Data are expressed as means ± SEM. LV, left ventricular; IVSd, interventricular septal thickness at end diastole; IVSs, interventricular septal thickness at end systole; LVIDd, left ventricular internal dimension at end diastole; LVIDs, left ventricular internal dimension at end systole; LVPWd, left ventricular posterior wall thickness at end diastole; LVPWs, left ventricular posterior wall thickness at end systole; FS, fractional shortening.*$p < 0.05$ versus sham group treated with vehicle; #$p < 0.05$ versus experimental group.

antagomir-mediated silencing mildly improved cardiac remodeling and differentially restored cardiac contractility, PPARδ expression, and key genes involved in fatty energy metabolism.

miR-199a∼214 Silencing Attenuates Cardiac Remodeling and Dysfunction

Next, we intervened in *miR-199a∼214* induction in cardiac disease conditions by subjecting mice to transverse aortic constriction pressure overload for 6 weeks and treating them with antagomirs for both *miR-199a* and *miR-214* for 3 consecutive days at 3-week intervals (Figure 4A). To ensure equal pressure gradients among the experimental groups, noninvasive pressure gradients across the transverse aorta were measured (Figure 4B). Vehicle-treated mice showed substantial cardiac enlargement upon biomechanical stress (Figure 4C), whereas antagomir-199a∼214-treated mice displayed significantly reduced heart weights (Figure 4D). Sham-operated mice treated with vehicle or antagomir-199a∼214 showed no signs of histopathology (Figure 4C). In contrast, cardiac tissue of vehicle-treated mice subjected to pressure overload displayed hypertrophied myofibers, myocyte disarray, and interstitial fibrosis, while mice treated with antagomir-199a∼214 displayed normal myocyte arrangement and significantly reduced hypertrophy and fibrosis (Figure 4C; Figure S4A). Analysis of cardiac function by M-mode echocardiography at 6 weeks showed an increase in LVID and a proportional decrease in systolic contractility (FS) in mice subjected to pressure overload and treated with vehicle (Figures 4E–4G; Table 2). Importantly, treatment with antagomir-199a∼214 derepressed PPARδ levels even in sham-operated animals and restored PPARδ expression following hemodynamic stress (Figures 4H and 4I), but did not influence PPARα expression (Figure S4B), further underscoring a specific role for PPARδ. To analyze the effect of antagomir treatment on metabolism in these hearts, we performed RT-PCRs for both fatty acid and glucose marker genes. Neither cardiac pressure overload nor antagomir-199a∼214 treatment altered the expression of genes implicated in glucose metabolism, including those encoding *solute carrier family 2 facilitated glucose transporter member 1* and *member 4* (*Slc2a1*, *Slc2a4*) and *hexokinase 1* (*Hk1*), in mouse hearts exposed to pressure overload (Figure 4J). In contrast, cardiac pressure overload induced pronounced changes in key genes involved in fatty acid metabolism, including *acyl-coenzyme A dehydrogenase, long chain* (*Acadl*) and *Acadm*, indicating restoration of fatty acid metabolism (Figure 4K).

miR-199a∼214 Silencing Restores Mitochondrial Fatty Acid Metabolism

Mitochondria play a crucial role in maintaining the energy homeostasis in the heart muscle (Marin-Garcia et al., 2001). Since in vivo antagomir-based silencing of *miR-199a* and *miR-214* resulted in a restoration of PPARδ expression and genes involved in fatty acid metabolism, we investigated whether mitochondrial ultrastructure was influenced. Transmission electron microscopy (TEM) assessment of heart sections showed salient mitochondrial disarray in pressure-overloaded mouse hearts (Figure 5A). Treatment with antagomir-199a∼214 normalized mitochondrial alignment in mice and restored I band width (Figure 5A), with unaltered expression of mitochondrial complex I–V components in pressure overload-induced cardiac dysfunction (Figure 5B; Figure S5A). We next assessed mitochondrial respiration in isolated cardiac mitochondria, fueled by two types of substrates: the carbohydrate-derived substrate pyruvate and the fatty acid-derived substrate palmitoyl-CoA (in the presence of carnitine) (Hoeks et al., 2010). Briefly, after the addition of substrate, maximal ADP-stimulated (state 3) respiration was determined. Subsequently, the leak rate (i.e., the respiratory rate in the presence of the ATP-synthase inhibitor oligomycin [state 4]) and the maximal respiratory capacity (i.e., the respiratory rate after addition of the chemical uncoupler FCCP [state U]) were assessed. These respiratory analyses revealed clear

(I) Quantification of GAPDH-corrected protein levels of PPARδ.
(J) Real-time PCR analysis of transcript abundance for glucose metabolism marker genes (J) and fatty acid metabolism marker genes (K) in mice hearts after 6 weeks of sham or TAC surgery, treated with vehicle or antagomirs. *$p < 0.05$ versus corresponding control group; #$p < 0.05$ versus corresponding experimental group (error bars are SEM). See also Figure S4.

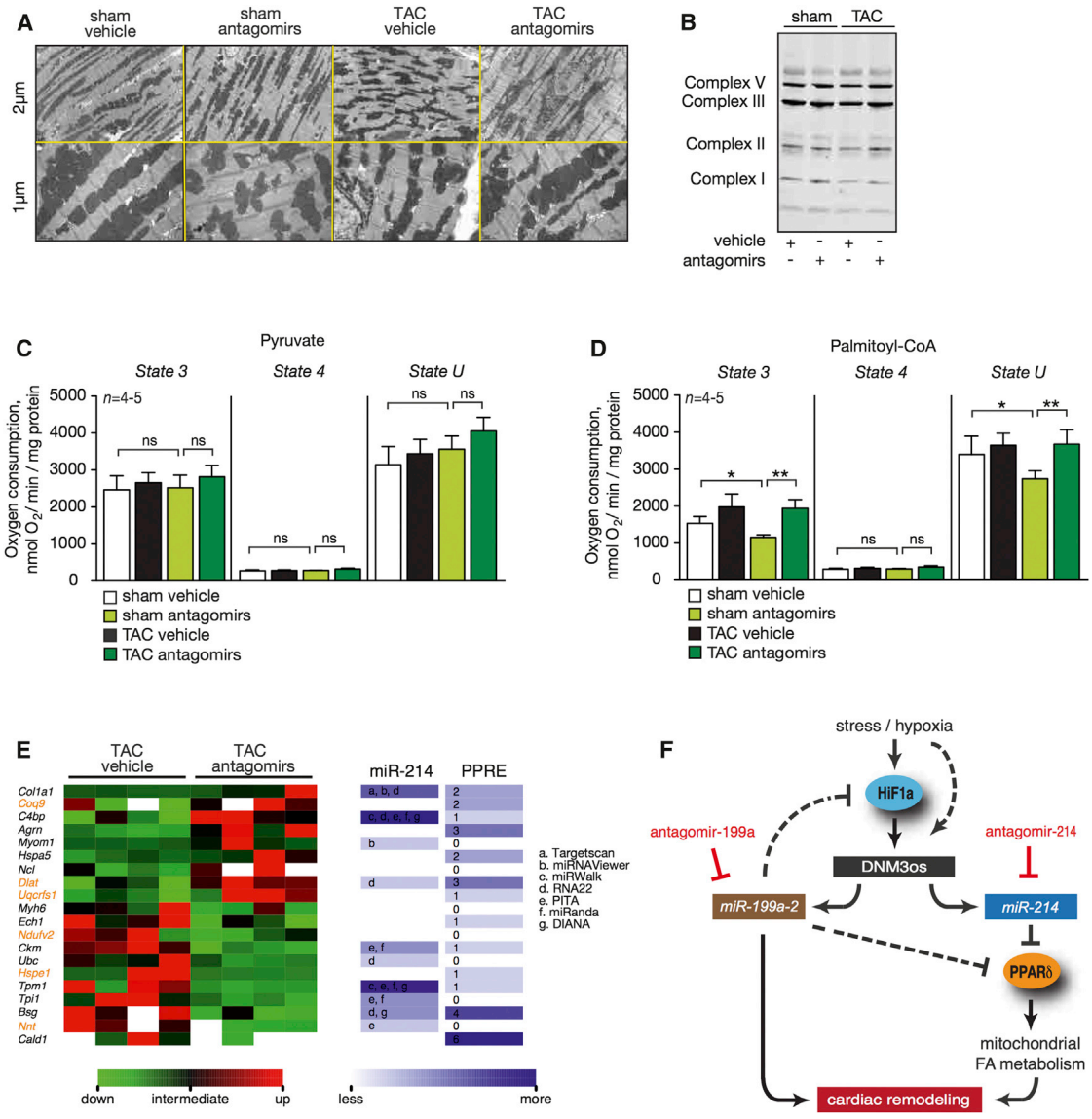

Figure 5. *miR-199a∼214* Silencing Preserves Mitochondrial Ultrastructure and Restores Fatty Acid Oxidation

(A) Transmission electron microscopy of heart sections from mice after 6 weeks of sham or TAC surgery, treated with vehicle or antagomirs.

(B) Western blot analysis using a cocktail of monoclonal antibodies, directed against various proteins of the electron transport chain (ETC) complexes of mitochondria from mice hearts after 6 weeks of sham or TAC surgery, treated with vehicle or antagomirs.

(C and D) Oxygen flux in mitochondria isolated from mouse cardiac tissue after 6 weeks of sham or TAC surgery, treated with vehicle or antagomirs. ADP-driven (state 3) and uncoupled (state U) oxygen flow was measured in the presence of pyruvate (C) and palmitoyl-CoA + carnitine (D) in mitochondria.

(E) Differentially expressed proteins detected by cardiac proteomics and computational analysis of the potential *miR-214* seed regions presence and/or the conserved number of PPRE sites present in the 10 kb promoter region. Depicted in orange are mitochondrial located genes.

(F) Model depicting the activation of hypoxia-mediated expression of the *miR-199a∼214* cluster under cardiac stress via the Hif1α/Twist1 pathway, leading to the targeting and subsequent downregulation of PPARδ. This results in perturbed mitochondrial fitness and reduced fatty acid metabolism. Antagomir-mediated silencing of *miR-199a* and *miR-214* derepresses PPARδ expression and normalizes cardiac energy homeostasis. *$p < 0.05$ versus corresponding control group; #$p < 0.05$ versus corresponding experimental group (error bars are SEM). See also Figure S5 and Table S2.

substrate-dependent changes in the mitochondrial oxidative capacity of the heart upon pressure overload and treatment with antagomir-199a∼214 (Figures 5C and 5D). Thus, when isolated cardiac mitochondria were fueled with the carbohydrate-derived substrate pyruvate, ADP-stimulated, oligomycin-insensitive as well as FCCP-induced respiration was similar across all groups (Figure 5C). On the other hand, pressure overload considerably reduced mitochondrial fatty acid oxidative capacity, as evidenced by a significant reduction in both the ADP-stimulated (−25%) and the maximally uncoupled respiration (−20%) upon the fatty acid substrate palmitoyl-CoA (Figure 5D). The leak rate (state 4 respiration) remained unaffected by pressure overload. Interestingly, the reduced fatty acid oxidative capacity upon pressure overload was completely restored by

antagomir-based silencing of the miRNA cluster *miR-199a∼214*, indicating that both ADP-stimulated and the maximally uncoupled respiration rate upon palmitoyl-Coa + carnitine was similar to the respective respiration rates observed in control animals. Single microRNAs likely simultaneously influence expression of up to 100 target genes (Hu et al., 2012). Given the strong restoration of mitochondrial fatty acid oxidative capacity and cardiac contractility of the hemodynamically challenged heart achieved by antagomir-199a∼214, we interrogated (using an unbiased proteomics screen) whether additional proteins were influenced either directly by silencing *miR-199a∼214* or indirectly by reactivation of PPARδ (Table S2). Accordingly, we detected an additional 20 differentially expressed proteins (five of which were mitochondrial) in pressure-overloaded hearts upon *miR-199a∼214* silencing, many of which harbored potential *miR-199a* (Figure S5B) or *miR-214* seed regions and/or contained PPAR response elements (PPREs) in their promoter region (Figure 5E), suggesting that *miR-199a∼214* silencing provokes specific alterations on the cardiac mitochondrial proteome in addition to PPARδ derepression. Altogether, our data suggest a mechanism whereby myocardial hypoxia, a characteristic of heart failure, induces expression of members of the miRNA cluster *miR-199a∼214* that actively downregulate several mitochondrial and cardiac targets including PPARδ, provoking a switch toward a glycolytic metabolic profile that contributes to heart failure (Figure 5F).

DISCUSSION

Although the regulation of metabolism is modulated by a variety of factors, the molecular mechanisms that drive the metabolic shift in the failing heart are still incompletely understood. The hemodynamically challenged myocardium exhibits a return to the fetal metabolic pattern that is hallmarked by impaired mitochondrial fatty acid oxidation and a shift to further reliance on glucose metabolism (Rajabi et al., 2007; Razeghi et al., 2001). Here, we propose a mechanism that integrates two characteristics of heart failure, hypoxia and a metabolic shift toward glycolysis, involving a microRNA cluster and a variety of target genes including PPARδ. We demonstrate that under hemodynamic stress, regional hypoxia in the heart activates *DNM3os*, a noncoding RNA transcript that harbors the miRNA cluster *miR-199a∼214*, in a HIF-dependent and/or HIF-independent manner. As one mechanistic explanation, the miRNA-mediated repression of PPARδ activity participates in a specific defect in mitochondrial respiration using fatty acids as substrate, resulting in a metabolic shift of the heart from predominant reliance on fatty acid utilization in the healthy myocardium toward increased reliance on glucose metabolism in the failing heart.

Recently, Gan and colleagues demonstrated that muscle-specific overexpression of PPARδ increased glucose oxidation in mitochondria through the reprogramming of glucose utilization pathways via interaction with the exercise-inducible AMP-activated protein kinase (AMPK) and myocyte enhancer factor 2A (MEF2A) (Gan et al., 2011). This effect may be selective for skeletal muscle, given that in our study we did not observe enhanced glucose utilization after reactivation of PPARδ in the hemodynamically stressed heart, but further lend evidence toward a role for PPARδ in the regulation of mitochondrial fueling. Targeted expression of an activated form of PPARδ in skeletal muscle induced a muscle fiber type switch, hereby conferring resistance to obesity and improved metabolic profiles, in part through increased mitochondrial function (Wang et al., 2004). Furthermore, conditional transgenic mice expressing a constitutively active form of PPARδ in cardiomyocytes displayed enhanced mitochondrial capacity at baseline and under conditions of pressure overload (Liu et al., 2011). In contrast, Wang et al. (2010) demonstrated that inducible gene targeting of PPARδ in the adult heart resulted in decreased mitochondrial function, concomitant with a hypertrophic response and decreased cardiac function. These data confirm our findings that restoring PPARδ levels in the heart maintains oxidative capacity of mitochondria and protects against heart failure. Conversely, our proteomics analysis of the *miR-199a∼214*-silenced myocardium has given us a first unbiased indication of additional factors further involved in the phenotypic changes we observed. As expected, a large number of them are mitochondria specific (*Coq9*, *Dlat*, *Uqcrfs1*, *Ndufv2*, *Hspe1*, and *Nnt*); however, their precise regulation by this pathway remains to be experimentally validated. As a first attempt to elucidate their potential dependency on a *miR-199a∼214*/PPARδ circuitry, we identified a number of potential PPREs as well as a number of potential binding sites for *miR-199a* and/or *miR-214*. These data suggest possible first or second degree interactions with our proposed mechanism and open up future studies to elucidate their function in cardiac energy metabolism.

As a key determinant of progression to heart failure, hypoxia is postulated to be a driving force for adverse cardiac remodeling. Pressure overload and ischemia often occur together clinically, as in patients with hypertension and coronary disease. As *miR-214* was recently demonstrated to act as a regulator of cardiomyocyte Ca^{2+} homeostasis and survival during acute cardiac ischemia-reperfusion injury (Aurora et al., 2012), the possible use of future *miR-214* therapeutics may be of more benefit in chronic cardiac (hypertrophic) remodeling processes rather than acute cardiac ischemic conditions. Indeed, pathologically hypertrophied hearts show significant decreased capillary density and associated hypoxia (Friehs et al., 2004). In a mouse model with cardiomyocyte-restricted deletion of the von Hippel-Lindau protein (VHL), a component of the E3 ubiquitin ligase that inhibits Hif1α, chronic activation of the Hif1α hypoxia response pathway is observed (Lei et al., 2008), resulting in progressive cardiac degeneration with lipid accumulation and decreased mitochondrial number leading to severe heart failure. Next to its role in modulating the fate of mesenchymal cell population during development, Twist1 has been also implicated in a wide range of neoplasias, including gastric, liver, and breast cancers (Karreth and Tuveson, 2004; Mironchik et al., 2005; Niu et al., 2007). Analysis of Twist1 expression showed a ubiquitous expression in various mouse tissues with diverse expression patterns, with relatively high expression in the cardiac ventricle (Lu et al., 2011), which is in line with the proposed regulatory role for *Dnm3os* expression. *Dnm3os*-deficient mice display defects in skeletal formation and body growth during embryonic development (Watanabe et al., 2008).

Taken together, our data show that *miR-199a* and *miR-214* play a pivotal role in PPARδ-mediated regulation of cardiac mitochondrial substrate fluxes with impact on cardiac structure and

function, resulting in a metabolic shift of the heart from predominant reliance on fatty acid utilization in the healthy myocardium toward increased reliance on glucose metabolism in the failing heart. Our observations indicate that human heart failure arises from derangements in gene regulatory circuits, where molecular understanding of these circuits will aid in predicting sites of therapeutic intervention.

EXPERIMENTAL PROCEDURES

Human Heart Samples

Tissue was taken from the left ventricular free wall of patients with end-stage heart failure secondary to ischemic heart disease or from patients undergoing heart transplantation because of terminal heart failure. Control tissue was taken from the left ventricular free wall of refused donor hearts.

Mouse Models

Mouse models included *Dnm3os*^{lacZ} mice (Watanabe et al., 2008), Hif1$\alpha^{F/F}$ mice (Ryan et al., 1998) interbred with myosin light chain 2v (MLC2v)-Cre mice (Chen et al., 1998) (Krishnan et al., 2009), and PPAR$\delta^{F/F}$ mice (Jackson Laboratories) interbred with mice harboring a tamoxifen-regulated form of Cre recombinase (MerCreMer) under control of the murine *Myh6* promoter (Sohal et al., 2001). All protocols were performed according to institutional guidelines and approved by local Animal Care and Use Committees.

Aortic Banding and Transthoracic Echocardiography

Transverse aortic constriction or sham surgery was performed in 2- to 3-month-old BL6CBAF1 mice by subjecting the aorta to a defined 27G constriction between the first and second truncus of the aortic arch as described previously (Bourajjaj et al., 2008; Rockman et al., 1991). Noninvasive, Doppler echocardiographic analysis was performed as described previously in detail (da Costa Martins et al., 2010).

Antagomir Administration

Antagomirs, 20–23 nt long RNA oligos complementary to *miR-199a* or *miR-214*, were purchased from Fidelity Systems or Integrated DNA Technologies and synthesized essentially as previously described (Krützfeldt et al., 2005), except that cholesterol was linked through a hydroxyprolinol linkage. All antagomirs were 2′-Ome modified, contained a 3′ cholesterol-TEG (15 atom triethylene glycol), 2 phosphorothioate (PT) bonds at the very first 5′ end, and PT bonds between the last 3′ bases. All antagomirs were HPLC purified and desalted before use.

Northern Blot Analysis

Northern blot analysis was performed as described previously (da Costa Martins et al., 2010) using 3′-digoxigenin-labeled locked nucleic acid oligonucleotides for *hsa-miR-199a*, *hsa-miR-214*, *mmu-miR-199a*, *mmu-miR-214*, or U6 small nuclear RNA (*Rnu6-2*) and detected with an antibody to 3′-digoxigenin (Roche).

MicroRNA and mRNA Real-Time PCR

Primer sequences are described in Table S3. Real-time PCR was performed using miScript SYBR Green PCR Kit (QIAGEN) on a Bio-Rad iCycler.

Primary Cardiomyocytes, Transient Transfections, and Luciferase Reporter Assays

Cardiomyocyte cultures were isolated by enzymatic dissociation of 1- to 2-day-old neonatal rat hearts, as described previously (De Windt et al., 2000), and transfected with *miR-199a*, *miR-214*, or scrambled-miR precursor molecules (Ambion) using oligofectamine (Invitrogen). Human embryonic kidney (HEK) 293 cells were transfected with pMIR reporter plasmids harboring the 3′ UTR of human PPARδ using FuGENE 6 (Roche) reagent, followed by transfection with *miR-199a*, *miR-214*, or scrambled miR precursor molecules using oligofectamine. For cotransfection assays, pGL3-Dnm3os promoter constructs were cotransfected with constructs expressing a stabilized form of Hif1α and/or Twist1. pRL-TK, containing the thymidine kinase promoter driving *Renilla* luciferase, was included to correct for transfection efficiency.

Western Blot Analysis

Immunoprecipitation, SDS PAGE electrophoresis, and blotting were performed as described previously (De Windt et al., 2000). Primary antibodies that were used for western blotting include polyclonal anti-PPAR-delta (Abcam), anti-PPAR-alpha (Abcam), monoclonal anti-GAPDH (Chemicon), and monoclonal total OXPHOS cocktail (MitoSciences), followed by corresponding horseradish peroxidase (HRP)-conjugated secondary antibodies and enhanced chemiluminescence (ECL) detection.

Histological Analysis and Immunofluorescence Microscopy

Hearts were arrested in diastole, paraffin embedded, sectioned at 4 μm, and stained with fluorescein isothiocyanate (FITC)-labeled wheat germ agglutinin (WGA), hematoxylin and eosin (H&E), Sirius red, or biotinylated Griffonia simplicifolia lectin I (GS-I) to visualize cardiac vascularization.

Isolation of Cardiac Mitochondria and Mitochondrial Respirometry

Cardiac tissue was processed for mitochondrial isolation by mechanical Potter homogenization, repeated centrifugation, and gentle resuspension. Mitochondrial respiratory rates were analyzed using an oxygraph (OROBOROS Instruments) (Hoeks et al., 2010).

Proteomics Analysis

Cardiac tissue was diced, PBS washed with proteinase inhibitors (Sigma-Aldrich), and incubated with 0.1% SDS, and the SDS solution was stored frozen. Next, samples were incubated with 4 M guanidine hydrochloride with proteinase inhibitors, proteins were precipitated by centrifugation, and the pellets were kept at −20°C. The gel bands were subjected to in-gel digestion with trypsin, and tryptic peptides were separated on a Nanoflow LC System (Dionex UltiMate 3000), eluted with a 40 min gradient, and the column (Dionex PepMap C18) was coupled to a nanospray source (PicoView). Spectra were collected from an ion trap mass analyzer (LTQ Orbitrap XL). Tandem mass spectrometry (MS/MS) was performed on the top six ions in each MS scan using the data-dependent acquisition mode with dynamic exclusion enabled. MS spectra were separately analyzed in MaxQuant Software. To construct a MS/MS peak list file, up to the top eight peaks per 100 Da window were extracted and submitted to search against a concatenated forward and reverse version of the UniProtKB/Swiss-Prot mouse database. A principal component analysis was performed using the normalized high/low ratios of all proteins from all samples. Significant differences were identified using the Bioconductor limma package and Bayesian statistics to moderate variance across proteins and calculate a p value.

Statistical Analysis

The results are presented as mean ± SEM. All statistical analyses were performed with Prism software (GraphPad), consisting of an ANOVA test followed by Tukey's post hoc test when group differences were detected at the 5% significance level or Student's t test when comparing two experimental groups. Differences were considered significant when $p < 0.05$.

SUPPLEMENTAL INFORMATION

Supplemental Information includes Supplemental Experimental Procedures, five figures, and three tables and can be found with this article online at http://dx.doi.org/10.1016/j.cmet.2013.08.009.

ACKNOWLEDGMENTS

We gratefully acknowledge members of the De Windt laboratory for helpful discussions and NingQing Liu, Joost Luiken, Natasja Kisters, and Javier Barallobre-Barreiro for technical support. P.D.C.M. was supported by a Leducq Career Development Award; the Netherlands Heart Foundation program grant NHS 2010B261, and Meervoud grant 836.12.001 from the Netherlands Organization for Health Research and Development (ZonMW). L.D.W. and Y.P. acknowledge support from the Center for Translational Molecular Medicine (CTMM)-TRanslational Initiative on Unique and novel strategies for Management of Patients with Heart failure (TRIUMPH) and *the Netherlands CardioVascular Research Initiative*: the Dutch Heart Foundation, Dutch Federation of University Medical Centers, ZonMW, and the Royal Netherlands Academy of

Sciences. L.D.W. was further supported by a VIDI award 917-863-72 and TOP grant 912-04-017 from the ZonMW; the Dutch Heart Foundation program grant NHS2007B167; the Fondation Leducq Transatlantic Network of Excellence program 08-CVD-03; and grant 311549 from the European Research Council (ERC). H.e.A., S.L., E.D., J.H., B.v.B., M.M.G.v.d.H., A.-S.A., M.B., and S.O. performed experiments. K.B., E.A.M., S.L., and A.S. analyzed proteomics data. J.C.S., J.K., M.V., and W.K. provided reagents and models. H.e.A., S.L., E.D., M.M., Y.M.P., P.A.d.C.M., P.S., and L.J.D.W. analyzed data and designed the study. H.e.A, S.L., P.A.d.C.M., and L.J.D.W. wrote the manuscript. H.e.A., S.L., and E.D. contributed equally as joint first authors.

Received: June 24, 2012
Revised: June 16, 2013
Accepted: August 7, 2013
Published: September 3, 2013

REFERENCES

Aurora, A.B., Mahmoud, A.I., Luo, X., Johnson, B.A., van Rooij, E., Matsuzaki, S., Humphries, K.M., Hill, J.A., Bassel-Duby, R., Sadek, H.A., and Olson, E.N. (2012). MicroRNA-214 protects the mouse heart from ischemic injury by controlling Ca^{2+} overload and cell death. J. Clin. Invest. *122*, 1222–1232.

Barak, Y., Liao, D., He, W., Ong, E.S., Nelson, M.C., Olefsky, J.M., Boland, R., and Evans, R.M. (2002). Effects of peroxisome proliferator-activated receptor delta on placentation, adiposity, and colorectal cancer. Proc. Natl. Acad. Sci. USA *99*, 303–308.

Barger, P.M., and Kelly, D.P. (2000). PPAR signaling in the control of cardiac energy metabolism. Trends Cardiovasc. Med. *10*, 238–245.

Bourajjaj, M., Armand, A.S., da Costa Martins, P.A., Weijts, B., van der Nagel, R., Heeneman, S., Wehrens, X.H., and De Windt, L.J. (2008). NFATc2 is a necessary mediator of calcineurin-dependent cardiac hypertrophy and heart failure. J. Biol. Chem. *283*, 22295–22303.

Burkart, E.M., Sambandam, N., Han, X., Gross, R.W., Courtois, M., Gierasch, C.M., Shoghi, K., Welch, M.J., and Kelly, D.P. (2007). Nuclear receptors PPARbeta/delta and PPARalpha direct distinct metabolic regulatory programs in the mouse heart. J. Clin. Invest. *117*, 3930–3939.

Chen, J., Kubalak, S.W., and Chien, K.R. (1998). Ventricular muscle-restricted targeting of the RXRalpha gene reveals a non-cell-autonomous requirement in cardiac chamber morphogenesis. Development *125*, 1943–1949.

Cheng, L., Ding, G., Qin, Q., Huang, Y., Lewis, W., He, N., Evans, R.M., Schneider, M.D., Brako, F.A., Xiao, Y., et al. (2004). Cardiomyocyte-restricted peroxisome proliferator-activated receptor-delta deletion perturbs myocardial fatty acid oxidation and leads to cardiomyopathy. Nat. Med. *10*, 1245–1250.

da Costa Martins, P.A., Bourajjaj, M., Gladka, M., Kortland, M., van Oort, R.J., Pinto, Y.M., Molkentin, J.D., and De Windt, L.J. (2008). Conditional dicer gene deletion in the postnatal myocardium provokes spontaneous cardiac remodeling. Circulation *118*, 1567–1576.

da Costa Martins, P.A., Salic, K., Gladka, M.M., Armand, A.S., Leptidis, S., el Azzouzi, H., Hansen, A., Coenen-de Roo, C.J., Bierhuizen, M.F., van der Nagel, R., et al. (2010). MicroRNA-199b targets the nuclear kinase Dyrk1a in an auto-amplification loop promoting calcineurin/NFAT signalling. Nat. Cell Biol. *12*, 1220–1227.

De Windt, L.J., Lim, H.W., Haq, S., Force, T., and Molkentin, J.D. (2000). Calcineurin promotes protein kinase C and c-Jun NH2-terminal kinase activation in the heart. Cross-talk between cardiac hypertrophic signaling pathways. J. Biol. Chem. *275*, 13571–13579.

Di Lisa, F., Canton, M., Menabò, R., Kaludercic, N., and Bernardi, P. (2007). Mitochondria and cardioprotection. Heart Fail. Rev. *12*, 249–260.

Friehs, I., Moran, A.M., Stamm, C., Choi, Y.H., Cowan, D.B., McGowan, F.X., and del Nido, P.J. (2004). Promoting angiogenesis protects severely hypertrophied hearts from ischemic injury. Ann. Thorac. Surg. *77*, 2004–2010, discussion 2011.

Gan, Z., Burkart-Hartman, E.M., Han, D.H., Finck, B., Leone, T.C., Smith, E.Y., Ayala, J.E., Holloszy, J., and Kelly, D.P. (2011). The nuclear receptor PPARβ/δ programs muscle glucose metabolism in cooperation with AMPK and MEF2. Genes Dev. *25*, 2619–2630.

Giordano, F.J. (2005). Oxygen, oxidative stress, hypoxia, and heart failure. J. Clin. Invest. *115*, 500–508.

Hoeks, J., van Herpen, N.A., Mensink, M., Moonen-Kornips, E., van Beurden, D., Hesselink, M.K., and Schrauwen, P. (2010). Prolonged fasting identifies skeletal muscle mitochondrial dysfunction as consequence rather than cause of human insulin resistance. Diabetes *59*, 2117–2125.

Hu, Y., Matkovich, S.J., Hecker, P.A., Zhang, Y., Edwards, J.R., and Dorn, G.W., 2nd. (2012). Epitranscriptional orchestration of genetic reprogramming is an emergent property of stress-regulated cardiac microRNAs. Proc. Natl. Acad. Sci. USA *109*, 19864–19869.

Karreth, F., and Tuveson, D.A. (2004). Twist induces an epithelial-mesenchymal transition to facilitate tumor metastasis. Cancer Biol. Ther. *3*, 1058–1059.

Krishnan, J., Suter, M., Windak, R., Krebs, T., Felley, A., Montessuit, C., Tokarska-Schlattner, M., Aasum, E., Bogdanova, A., Perriard, E., et al. (2009). Activation of a HIF1alpha-PPARgamma axis underlies the integration of glycolytic and lipid anabolic pathways in pathologic cardiac hypertrophy. Cell Metab. *9*, 512–524.

Krützfeldt, J., Rajewsky, N., Braich, R., Rajeev, K.G., Tuschl, T., Manoharan, M., and Stoffel, M. (2005). Silencing of microRNAs in vivo with 'antagomirs'. Nature *438*, 685–689.

Lei, L., Mason, S., Liu, D., Huang, Y., Marks, C., Hickey, R., Jovin, I.S., Pypaert, M., Johnson, R.S., and Giordano, F.J. (2008). Hypoxia-inducible factor-dependent degeneration, failure, and malignant transformation of the heart in the absence of the von Hippel-Lindau protein. Mol. Cell. Biol. *28*, 3790–3803.

Leptidis, S., El Azzouzi, H., Lok, S.I., de Weger, R., Olieslagers, S., Kisters, N., Silva, G.J., Heymans, S., Cuppen, E., Berezikov, E., et al. (2013). A deep sequencing approach to uncover the miRNOME in the human heart. PLoS ONE *8*, e57800.

Liu, J., Wang, P., Luo, J., Huang, Y., He, L., Yang, H., Li, Q., Wu, S., Zhelyabovska, O., and Yang, Q. (2011). Peroxisome proliferator-activated receptor β/δ activation in adult hearts facilitates mitochondrial function and cardiac performance under pressure-overload condition. Hypertension *57*, 223–230.

Loebel, D.A., Tsoi, B., Wong, N., and Tam, P.P. (2005). A conserved noncoding intronic transcript at the mouse Dnm3 locus. Genomics *85*, 782–789.

Lu, S., Nie, J., Luan, Q., Feng, Q., Xiao, Q., Chang, Z., Shan, C., Hess, D., Hemmings, B.A., and Yang, Z. (2011). Phosphorylation of the Twist1-family basic helix-loop-helix transcription factors is involved in pathological cardiac remodeling. PLoS ONE *6*, e19251.

Marin-Garcia, J., Goldenthal, M.J., and Moe, G.W. (2001). Mitochondrial pathology in cardiac failure. Cardiovasc. Res. *49*, 17–26.

Mironchik, Y., Winnard, P.T., Jr., Vesuna, F., Kato, Y., Wildes, F., Pathak, A.P., Kominsky, S., Artemov, D., Bhujwalla, Z., Van Diest, P., et al. (2005). Twist overexpression induces in vivo angiogenesis and correlates with chromosomal instability in breast cancer. Cancer Res. *65*, 10801–10809.

Niu, R.F., Zhang, L., Xi, G.M., Wei, X.Y., Yang, Y., Shi, Y.R., and Hao, X.S. (2007). Up-regulation of Twist induces angiogenesis and correlates with metastasis in hepatocellular carcinoma. J. Exp. Clin. Cancer Res. *26*, 385–394.

Rajabi, M., Kassiotis, C., Razeghi, P., and Taegtmeyer, H. (2007). Return to the fetal gene program protects the stressed heart: a strong hypothesis. Heart Fail. Rev. *12*, 331–343.

Razeghi, P., Young, M.E., Alcorn, J.L., Moravec, C.S., Frazier, O.H., and Taegtmeyer, H. (2001). Metabolic gene expression in fetal and failing human heart. Circulation *104*, 2923–2931.

Rey, S., and Semenza, G.L. (2010). Hypoxia-inducible factor-1-dependent mechanisms of vascularization and vascular remodelling. Cardiovasc. Res. *86*, 236–242.

Rockman, H.A., Ross, R.S., Harris, A.N., Knowlton, K.U., Steinhelper, M.E., Field, L.J., Ross, J., Jr., and Chien, K.R. (1991). Segregation of atrial-specific and inducible expression of an atrial natriuretic factor transgene in an in vivo

murine model of cardiac hypertrophy. Proc. Natl. Acad. Sci. USA *88*, 8277–8281.

Ryan, H.E., Lo, J., and Johnson, R.S. (1998). HIF-1 alpha is required for solid tumor formation and embryonic vascularization. EMBO J. *17*, 3005–3015.

Sabbah, H.N., Sharov, V.G., and Goldstein, S. (2000). Cell death, tissue hypoxia and the progression of heart failure. Heart Fail. Rev. *5*, 131–138.

Sohal, D.S., Nghiem, M., Crackower, M.A., Witt, S.A., Kimball, T.R., Tymitz, K.M., Penninger, J.M., and Molkentin, J.D. (2001). Temporally regulated and tissue-specific gene manipulations in the adult and embryonic heart using a tamoxifen-inducible Cre protein. Circ. Res. *89*, 20–25.

Tanaka, M., Ito, H., Adachi, S., Akimoto, H., Nishikawa, T., Kasajima, T., Marumo, F., and Hiroe, M. (1994). Hypoxia induces apoptosis with enhanced expression of Fas antigen messenger RNA in cultured neonatal rat cardiomyocytes. Circ. Res. *75*, 426–433.

Thum, T., Galuppo, P., Wolf, C., Fiedler, J., Kneitz, S., van Laake, L.W., Doevendans, P.A., Mummery, C.L., Borlak, J., Haverich, A., et al. (2007). MicroRNAs in the human heart: a clue to fetal gene reprogramming in heart failure. Circulation *116*, 258–267.

van Rooij, E., Sutherland, L.B., Liu, N., Williams, A.H., McAnally, J., Gerard, R.D., Richardson, J.A., and Olson, E.N. (2006). A signature pattern of stress-responsive microRNAs that can evoke cardiac hypertrophy and heart failure. Proc. Natl. Acad. Sci. USA *103*, 18255–18260.

van Rooij, E., Sutherland, L.B., Qi, X., Richardson, J.A., Hill, J., and Olson, E.N. (2007). Control of stress-dependent cardiac growth and gene expression by a microRNA. Science *316*, 575–579.

Wang, Y.X., Zhang, C.L., Yu, R.T., Cho, H.K., Nelson, M.C., Bayuga-Ocampo, C.R., Ham, J., Kang, H., and Evans, R.M. (2004). Regulation of muscle fiber type and running endurance by PPARdelta. PLoS Biol. *2*, e294.

Wang, P., Liu, J., Li, Y., Wu, S., Luo, J., Yang, H., Subbiah, R., Chatham, J., Zhelyabovska, O., and Yang, Q. (2010). Peroxisome proliferator-activated receptor delta is an essential transcriptional regulator for mitochondrial protection and biogenesis in adult heart. Circ. Res. *106*, 911–919.

Watanabe, T., Sato, T., Amano, T., Kawamura, Y., Kawamura, N., Kawaguchi, H., Yamashita, N., Kurihara, H., and Nakaoka, T. (2008). Dnm3os, a non-coding RNA, is required for normal growth and skeletal development in mice. Dev. Dyn. *237*, 3738–3748.

Yang, M.H., Wu, M.Z., Chiou, S.H., Chen, P.M., Chang, S.Y., Liu, C.J., Teng, S.C., and Wu, K.J. (2008). Direct regulation of TWIST by HIF-1alpha promotes metastasis. Nat. Cell Biol. *10*, 295–305.